PCCP

PAPER

View Article Online
View Journal | View Issue

Cite this: *Phys. Chem. Chem. Phys.*, 2014, **16**, 4699

Local geometric and electronic structures of gasochromic VO_x films†

Wei-Luen Jang,[a] Yang-Ming Lu,[b] Chi-Liang Chen,[c] Ying-Rui Lu,[ad] Chung-Li Dong,*[a] Ping-Hung Hsieh,[e] Weng-Sing Hwang,[e] Jeng-Lung Chen,[a] Jin-Ming Chen,[a] Ting-Shan Chan,[a] Jyh-Fu Lee[a] and Wu-Ching Chou[f]

Received 12th November 2013,
Accepted 16th January 2014

DOI: 10.1039/c3cp54773f

www.rsc.org/pccp

VO_x films were deposited by radio-frequency reactive magnetron sputtering from a vanadium target at room temperature. Local atomic and electronic structures of the films were then modified by thermal annealing. The oxidation state and structural and gasochromic properties of the films were elucidated by X-ray absorption spectroscopy. Analytical results indicate that the as-deposited VO_x films were amorphous with mixed V^{4+} and V^{5+} valences. The amorphous VO_x had a disordered and expanded lamellar structure resembling that of polymer-intercalated V_2O_5 gels. VO_x films were crystallized into orthorhombic V_2O_5 at 300 °C, and the lamellar structure was eliminated at 400 °C. Additionally, the gasochromic reaction reduced the vanadium valence *via* intervalence transitions between V^{5+} and V^{3+}. Moreover, removing the lamellar structure reduced the gasochromic rate, and the gasochromic reaction transformed the V_2O_5 crystalline phase irreversibly into an $H_{1.43}V_2O_5$ phase. Based on the results of this study, amorphous VO_x with a lamellar structure is recommended for use in H_2 gas sensors.

Introduction

Electrochromic thin film material is a rapidly growing field owing to its wide range of applications. Two highly promising commercial applications of this material are energy-saving window materials and hydrogen sensors. Buildings consume approximately 40% of all energy used in daily life, and humans spend an average of 80% to 90% of their lives indoors,[1] warranting significant improvements in the energy efficiency of buildings. Windows account for a significant amount of wasted energy in buildings; electrochromic windows represent a viable energy-saving solution.[2,3] One proposed electrochromic window is made of a laminated thin film structure, in which current is generated in the thin film battery when the sun shines on the window, which darkens it. Despite the unavailability of this technology, electrochromic films may serve this purpose in the future. Additionally, renewable energy resources have received considerable attention, owing to the global energy crisis and extreme climatic conditions worldwide. Hydrogen burns to form water, and no gas is responsible for global warming. Therefore, hydrogen is widely regarded as a promising alternative energy source to replace oil.[4,5] The risk of hydrogen exploding in air at concentrations as low as 4% poses a major obstacle to adopting hydrogen energy technology. Safely handling hydrogen is critical to successfully developing a hydrogen economy. Hydrogen leakages at storage or usage sites must be monitored continuously to ensure safety. Hydrogen sensors are characterized by their durability and reliability. Despite the use of electrochromic films in H_2 sensors, their reliable operation depends on replacing the liquid electrolyte regularly.[6] Developing a hydrogen sensor that consumes low power and requires negligible maintenance is thus of priority concern. One feasible approach fully exploits the gasochromic properties of electrochromic thin films.[7,8] These materials change color when exposed to hydrogen, allowing for the detection of hydrogen by monitoring the changes in their optical transmission. This approach is superior to measuring electrical conductivities for sensing, possibly causing a hydrogen explosion.[6]

Vanadium oxygen systems comprise many oxide phases, including VO, V_2O_3, VO_2, V_6O_{13}, V_3O_7, and V_2O_5. Of these, V_2O_5 has the highest oxidation state and is widely regarded as an intercalation host for Li or H cations. V_2O_5 has a diverse array of applications, including Li batteries,[9,10] optical H_2 sensors,[11–14]

[a] *National Synchrotron Radiation Research Center, Hsinchu 30076, Taiwan. E-mail: dong.cl@nsrrc.org.tw*
[b] *Department of Electrical Engineering, National University of Tainan, Tainan 70005, Taiwan*
[c] *Institute of Physics, Academia Sinica, Taipei 11529, Taiwan*
[d] *Program for Science and Technology of Accelerator Light Source, National Chiao Tung University, Hsinchu 30010, Taiwan*
[e] *Department of Materials Science and Engineering, National Cheng Kung University, Tainan 70101, Taiwan*
[f] *Department of Electrophysics, National Chiao Tung University, Hsinchu 30010, Taiwan*

† Electronic supplementary information (ESI) available. See DOI: 10.1039/c3cp54773f

and electrochromic devices.[15,16] V_2O_5 thin films are yellow in their bleached state, turning gray or black with the insertion of ions. V_2O_5 for use as an intercalation host is normally prepared using the sol–gel method.[17] Upon the slow removal of the solvent, V_2O_5 film becomes amorphous with an ordered stacking of V_2O_5 ribbons.[17] As is widely assumed, the lamellar structure provides a channel for the rapid intercalation of ion species. In crystalline V_2O_5,[18] phase transformations occur during intercalation and de-intercalation processes, subsequently forming irreversible γ and ω phases. These irreversible phases either yield an unsatisfactory cycle performance or reduce the capacity of thin-film Li batteries. In contrast, no phase transformation occurs in amorphous vanadium oxide during Li intercalation. Correspondingly, the structural properties are important to the intercalation properties of the films. Sensor films prepared by vacuum evaporation[19,20] are characterized by their sensitivity, easily controlled deposition parameters and uniformity,[21,22] allowing for a detailed study of the coloration mechanism with respect to their electronic and atomic structures. Growth parameters can be fine-tuned to optimize the thin film. Most studies investigate the optical properties of such films.[7,23,24] Absorption/transmittance spectra are examined to describe the optical properties of sensor films during reduction/oxidation.[23,25] Gasochromic V_2O_5 films have rarely been investigated. To our knowledge, no study has elucidated the gasochromic properties of sputtered vanadium oxide films in terms of atomic/electronic structures. The gasochromic switching of vanadium oxide is of great interest from both technological and fundamental perspectives. In this study, amorphous VO_x thin films are prepared by sputter deposition. Their film structures are modified by thermal annealing. Based on *in situ* X-ray absorption spectroscopy (XAS), the electronic and local atomic environments are investigated to determine the parameters for fabricating gasochromic films. Additionally, the overall gasochromic properties of sensor films are determined using the shapes of the XAS spectra. Moreover, exactly how the structural parameters affect the gasochromic reaction of the films is examined. Results of this study demonstrate that the amorphous VO_x film with a lamellar structure and with a locally distorted pyramid (Py) symmetry is highly promising for use in H_2 sensors.

Experimental

VO_x films were deposited on a Corning 1737 substrate by using a radio-frequency reactive magnetron sputtering system with a vanadium target. The working power was fixed at 150 W and the sputter deposition was performed at a gas pressure of 1.33 Pa in pure O_2. Thickness of the deposited films was controlled at 200 nm. The as-deposited VO_x films were then annealed at 200 (AA200), 300 (AA300), and 400 °C (AA400) in air for 5 min. Next, a thin (~5 nm) Pt layer was deposited on the as-deposited and annealed VO_x films as a hydrogen catalyst. During the gasochromic reaction, the films were exposed to pure hydrogen for 2 h at 101.325 kPa and 25 °C. Experiments involving synchrotron-based approaches were undertaken at the National Synchrotron Radiation Research Center (NSRRC), Hsinchu, Taiwan. The crystalline structures of the films were determined by grazing incidence X-ray diffraction (GIXRD) and X-ray powder diffraction (XRD) at BL01C2. The electronic and atomic structures of the as-deposited and annealed VO_x films were studied by XAS. The synchrotron XAS were recorded two to three times to ensure the data reliability and reproducibility (Fig. S1–S5, ESI†). The V $L_{2,3}$-edges and O K-edge XAS were recorded at the soft-X-ray beamline BL20A. A homemade flow gas cell was used to perform *in situ* (polarized) V K-edge XAS measurements. The angles of incidence between the photon beam and the sample surface were 20°, 45°, and 90°. V K-edge XAS spectra were collected at the hard-X-ray beamline BL17C. The resolutions for hard-X-ray and soft-X-ray spectroscopic measurements were set to 0.5 and 0.2 eV, respectively.

Results and discussion

Fig. 1 illustrates the GIXRD patterns of the as-deposited and annealed VO_x films. Reference samples of polycrystalline V_2O_5 (orthorhombic), VO_2 (B), and VO_2 (M) films were prepared. Fig. 1(a) shows their spectra. Crystalline V_2O_5 was obtained by thermally annealing as-deposited VO_x at 500 °C in air for 2 h. VO_2 (B) was obtained by thermally annealing as-deposited VO_x at 360 °C in a 90% Ar–10% H_2 mixture for 3 h. VO_2 (M) was obtained by annealing VO_2 (B) at 500 °C in N_2 for 1 h. Structures of the standards were confirmed by GIXRD. The as-deposited VO_x yielded only a broad peak at ~6°. This low-angle peak originated from the stacking structure along the *c*-axis and was indexed as (001).[26] The shift of the peak to a higher 2θ angle coincided with the decrease in the full width at half maximum (FWHM) when increasing the annealing temperature to 200 and 300 °C. Diffraction peaks that correspond to the orthorhombic V_2O_5 phase (JCPDS card no. 41-1426) were found at 300,

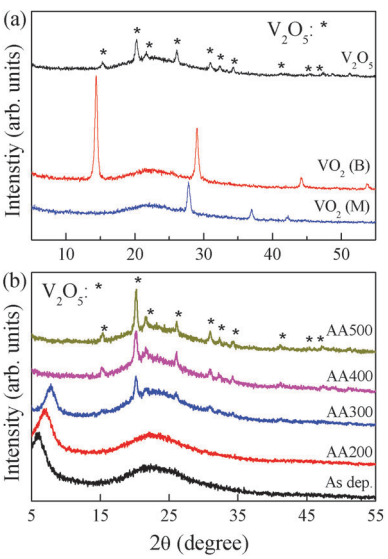

Fig. 1 GIXRD patterns of (a) reference samples and (b) as-deposited and annealed VO_x films.

400 and 500 °C. According to the GIXRD patterns, the as-deposited VO_x and AA200 were amorphous. Additionally, the films readily dissolved in water, yielding a clear yellowish solution, verifying the amorphous nature of the films, as suggested by Livage *et al.*[17,27] The broad peaks of the as-deposited VO_x, AA200, and AA300 are related to the (001) peaks of materials with lamellar structures.[17,28] Moreover, the interlayer distances determined from the Bragg's law are 14.7, 12.83, and 11.29 Å, respectively.

Many studies have attempted to improve the electrochemical properties of V_2O_5 xerogel powders by changing the procedure for drying bulk materials or adding the inert ceramic material.[17,26] The objective is to modify the final products morphologically and structurally to enhance their electrochemical performance, including their ionic conductivity. However, controlling the final product quality from the liquid solution is rather difficult. Herein, sputtered VO_x films were prepared and the annealing temperature was controlled to obtain different annealed films with different degrees of amorphicity. With only a few studies describing amorphous vanadium oxide films prepared by sputter deposition,[18,21,29] to our knowledge, no information is available on their lamellar structures. Similar lamellar structures have been identified in $V_2O_5{\cdot}nH_2O$ gels, which comprise ribbon-like species.[17] Previous studies have suggested that this ribbon-based structure is a bilayered structure.[30–32] A related study found ordered stacking of the V_2O_5 structure when the gel was deposited onto a flat surface with the slow removal of the solvent.[17] The XRD pattern of the ordered xerogel generally includes a strong (001) peak with other sets of (00*l*) peaks. The interlayer distance depends on the water content (11.5 Å for $V_2O_5{\cdot}1.8H_2O$ and 8.8 Å for $V_2O_5{\cdot}0.5H_2O$).[17,28] Additionally, the intercalation of polymers substantially reduces the (001) intensity and eliminates some (00*l*) peaks.[29,30] Intercalation also increases the interlayer distance and FWHM of the (001) peak. The vanadium oxide films in this study have interlayer distances that are comparable to (or even greater than) that in $V_2O_5{:}xH_2O$. However, these films do not contain water molecules since sputtering occurs in a vacuum and should not involve water. In $V_2O_5{:}xH_2O$, removing the water molecules reduces the interlayer distance. This effect was not observed in this study, which demonstrates that maintenance of the large interlayer distance does not depend on molecular water. The GIXRD pattern of as-deposited VO_x herein resembles that of polymer-modified V_2O_5 gels, implying that this large interlayer spacing arises from the intrinsic properties or some sputtered species are intercalated into the layers of as-deposited VO_x.

While using X-rays to promote electrons from core levels to partially filled and empty states, XAS spectroscopy is a local element-specific probe of the electronic and geometric structures of a material. This method is thus a highly effective means of studying vanadium oxide-based materials that exhibit various symmetry distortions and valence states. In a purely ionic representation of the V_2O_5 ground state, the O 2p orbital is completely filled (O^{2-}) whereas the V 3d state is unoccupied (V^{5+}, $3d^0$ configuration). The covalent V–O interaction causes a significant contribution of the O 2p orbitals above the Fermi level, in an energy region dominated by the V 3d orbitals. With perfect O_h symmetry, the V 3d orbitals are split into two sub-groups, *i.e.* t_{2g} at the lower energy and e_g at the higher one, by crystal field splitting. Deviations from the octahedral environment are particularly strong for V atoms in the V_2O_5 crystal structure and it is associated with further splitting of the 3d t_{2g} and 3d e_g orbitals. The t_{2g}-like orbital is split into the lower $3d_{xy}$ orbital component and the higher $3d_{xz}$ and $3d_{yz}$ orbital components; the e_g-like orbital is also split into $3d_{x^2-y^2}$ and $3d_{z^2}$ components. In this study, the electronic structure and vanadium valence of the as-deposited and annealed VO_x films were determined from the XAS spectra of the V L- and O K-edge, as shown in Fig. 2(a) and (b), respectively.

In the V L-edge XAS in Fig. 2(a), spin–orbital coupling splits the V 2p core hole into $2p_{3/2}$ and $2p_{1/2}$ levels, yielding the V L_3 and V L_2 edges at approximately 518 and 525 eV, which arise from $V2p_{3/2} \rightarrow$ V 3d and $V2p_{1/2} \rightarrow$ V 3d transitions, respectively. The spin orbit splitting between the L_3 and L_2 peaks is around 6.7 eV for the AA500 film, which is similar to that of single crystal V_2O_5.[33,34] Notably, the L_3 XAS of crystal V_2O_5 includes several recognizable features, A_2–D_2. As mentioned above, the peaks in the L_3 XAS arise mainly from the crystal field splitting of the final 3d orbitals. The nature of the L_2 transitions resembles that of the L_3 transitions. However, the spectral resolution in the V L_2-edge was lower than that in the V L_3-edge. The L_2 peak is broadened by a Coster–Kronig Auger decay process into a $2p_{3/2}$ hole, subsequently increasing the number of decay channels and ultimately shortening the lifetime of the excited state. Simultaneously, the peak is broadened by time–energy uncertainty. Therefore, the V L_2-edge is normally less informative than the L_3-edge in terms of elucidating the electronic structure.

Of the fine structures in the V L_3-edge of crystalline V_2O_5, the very weak A_2 feature in the low-energy range originates from the

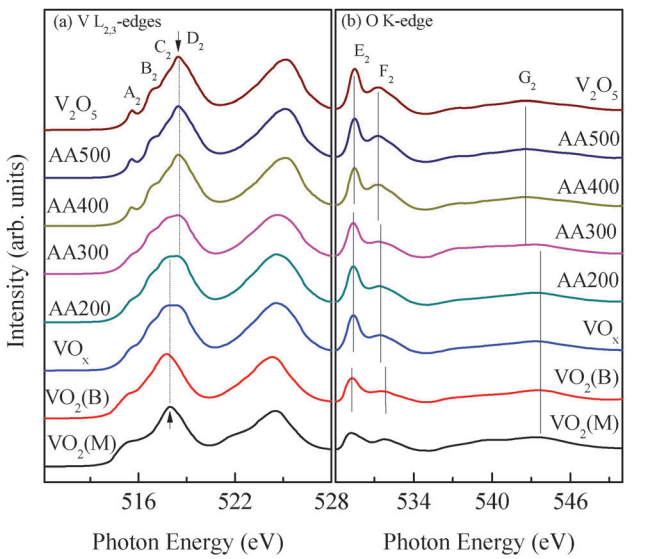

Fig. 2 (a) V 2p and (b) O 1s XAS spectra of as-deposited and annealed VO_x films and standards (VO_2 (M), VO_2 (B), and V_2O_5).

mixed configurations that arise from the transitions toward 3d orbitals dominated by both the central V atom and the V neighbor atoms. This feature can be described in terms of molecular orbitals that comprise both a central V $3d_{xy}$ component and 3d t_{2g}-like components of the neighboring V atoms.[35,36] Approximately 1.4 eV above A_2 is B_2, which is a transition that is characteristic of the other two t_{2g}-like components, $3d_{xz}$ and $3d_{yz}$. The increased intensity of this peak B_2 is caused by an increase in the 3d contribution of the excited V atoms relative to that of the peripheral V atoms in the final states.[35,36] The C_2 and D_2 peaks are associated with the e_g-like components. According to a finite cluster model calculation, the C_2 peak has a higher percentage of $3d_{x^2-y^2}$ character of the central V atom while the D_2 peak is derived from transitions that are primarily associated with the $3d_{z^2}$ component of that atom.[34,36] Although the assignments of peaks A_2 and B_2 contradict an earlier study that assigned them to transitions from V 2p to V 4s,[37] disordered vanadium oxides such as powdered and polycrystalline samples never generate two peaks A_2 and B_2. For single crystals, the shoulder is pronounced.[37,38] The smear of the fine structures can be viewed as an indicator of the degree of disorder. This disorder may affect the 3d contribution from the central and neighboring V atoms. Notably, the separation of C_2 and D_2 is less clear in the spectrum of the VO_x sample than in that of the crystalline V_2O_5 sample, probably owing to the higher degree of disorder in the first case.[34,38] Additionally, C_2 ($3d_{x^2-y^2}$) from VO_x and AA200 is more intense than that from crystalline V_2O_5 perhaps because the central V atom is closer to the basal plane; the $d_{x^2-y^2}$ component is thus stronger. Above results verify the amorphous nature of the as-prepared VO_x film and its crystallization upon thermal annealing, as revealed by GIXRD. This nature may also be owing to the association of V^{4+} with VO_2. In the V 2p XAS spectra, the L_3 peak of the VO_2 standards shifts to a lower photon energy than that of the V_2O_5 standard, as indicated by the upward and downward-pointing arrows in Fig. 2(a). The shift is owing to the increase in the occupancy of electrons, which enhances the screening of the core holes, thereby lowering the absorption energy. The L_3 main peaks of VO_x, AA200, and AA300 are relatively broad, and the energy range covers the L_3 main peaks of the VO_2 and V_2O_5 standards. Additionally, the characteristics of V^{4+} gradually disappear as the annealing temperature increases. The V 2p XAS spectra of AA400 and AA500 are almost the same as that of the V_2O_5 standard, which is consistent with the GIXRD results. Experimental results indicate that, in addition to the as-deposited VO_x films having a +4 and +5 mixed valence, thermal annealing reduces the amount of V^{4+}. The spectral profile depends not only on the charge state but also on the orbital symmetry, as revealed in greater detail by the O K-edge XAS discussed later.

Fig. 2(b) presents the O K-edge XAS. The O 2p orbitals are greatly mixed with the corresponding V 3d orbitals, giving rise to a widely spread and considerably intense absorption signal. This finding clearly indicates the significant covalent character of the V–O bonds in the film. The spectra of the all samples exhibit clear similarities, and each one can be divided into two regions. The first region is the pre-edge from the absorption edge up to 5–7 eV and includes two distinct structures at 529 (E_2) and 531 eV (F_2) that are split into O 2p–V 3d(t_{2g}) and O 2p–V 3d(e_g) states, respectively, by the crystal field effect. More specifically, the most intense peak at low energy in the O K pre-edge spectra has a t_{2g}-like structure and corresponds to the π interactions between the O $2p_{xy}$ levels and V $3d_{xy}$, $3d_{xz}$, and $3d_{yz}$ levels;[34,36] the high-energy e_g-like structure arises from σ interactions between O $2p_z$ orbitals and V $3d_{x^2-y^2}$ and $3d_{z^2}$ orbitals that point directly toward the oxygen ligands.[34,36] Accordingly, the pre-edge spectrum is highly sensitive to changes in the charge states and orbital symmetry upon thermal annealing. As is expected, the crystallographically distinct oxygen atoms differ slightly in the overlapping O 2p–V 3d hybridization, thereby affecting the spectral profile and orbital energy. Hence, the modification of the O K-edge upon thermal annealing is attributed to an increase in the number of crystallographically inequivalent oxygen sites. The second region appears at higher energies and exhibits a highly complex structure. This region is associated with the mixture of O 2p states with V 4sp states, and is pushed up in energy by the increase in strength of the O 2p–V 4sp interactions (peak G_2). The G_2 peak in VO_x, and AA200 is shifted to a higher energy than those of AA300, AA400 and AA500 because the 3d orbitals become more extended with an increasing electron occupancy, resulting in a greater overlap with the O 2p orbitals and a larger splitting. This finding implies that the valence is lower in VO_x and AA200 than the other films, which corresponds to the observed shift of the V L_3-edge in as-prepared or AA200 films to a lower energy.

According to Fig. 2(b), t_{2g} (E_2) and e_g (F_2) structures of the sputtered films are similar to those of the standards. Closely examining the energy separation, $\Delta E(E_{eg} - E_{t_{2g}})$, of these films reveals that the ΔE decreases with an increasing annealing temperature; in addition, their values equal that of V_2O_5 above 300 °C. The energy separation, ΔE, yields information about ligand-field splitting, which is influenced by the local coordination of vanadium atoms. As mentioned above, in O_h symmetry, the 3d orbital is split into t_{2g} and e_g states. In V_2O_5 with a C_{4v} crystal field, the t_{2g} orbital is further split into e (d_{xz}, and d_{yz}) and b_2 (d_{xy}) states; in addition the e_g orbital is split into a_1 (d_{z^2}) and b_1 ($d_{x^2-y^2}$) states.[39] Generally, $10D_q$ refers to the energy splitting between the t_{2g} and e_g orbitals, whereas $4D_s + 5D_t$ and $3D_s - 5D_t$ are the energy splits ΔEt_{2g} (e and b_2) and Δe_g (a_1 and b_1). Therefore, the energies of the e, b_2, a_1 and b_1 levels in C_{4v} symmetry are $6D_q + 2D_s - 6D_t$, $6D_q + 2D_s - 1D_t$, $-4D_q + 2D_s - 1D_t$, and $-4D_q - 1D_s + 4D_t$, respectively.[39] The energy separations ΔEt_{2g} (e and b_2) are too small to be resolved in the X-ray absorption spectrum, but they can be identified by the cluster model calculation with a single particle approximation.[39] Notably, Δe_g (a_1 and b_1) is approximately 1.4 eV, allowing for the contributions of (d_{z^2}) and ($d_{x^2-y^2}$) to be determined from the deconvoluted XAS spectrum.

Fig. 3 presents the deconvolution of the pre-edge region of the O K-edge. The inset displays the variations of the t_{2g} and e_g (d_{z^2} and $d_{x^2-y^2}$) states for all of the films. The inset shows changes in the relative weights of the d_{z^2} and $d_{x^2-y^2}$ structures,

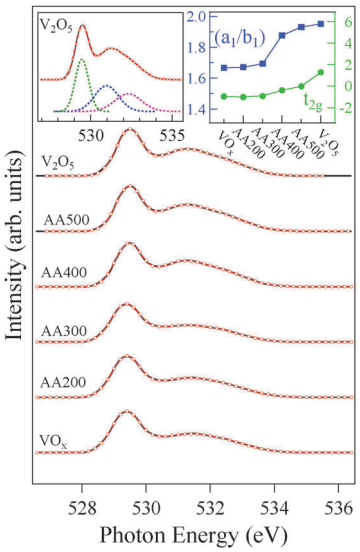

Fig. 3 Experimental pre-edge of O K-edge XAS for V_2O_5 and deposited VO_x films and those fitted by Gaussian profiles (red circle). Inset (left) shows the fitted data using Gaussian profiles for t_{2g} and e_g states. Inset (right) represents the integrated area of (a_1/b_1) and t_{2g} peaks.

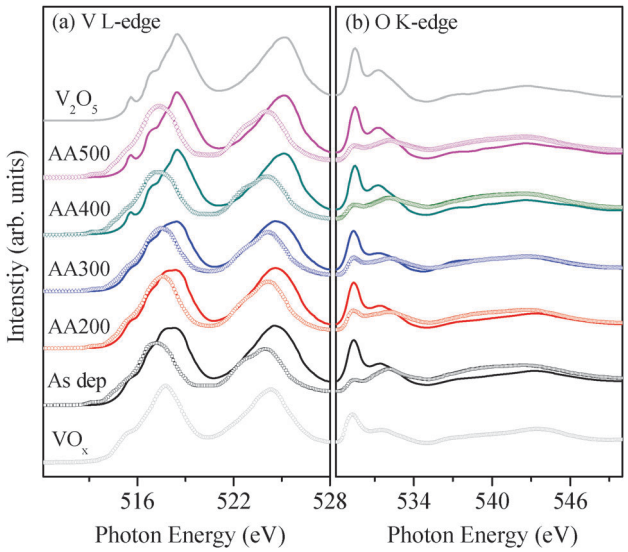

Fig. 4 (a) V $L_{2,3}$-edge and (b) O K-edge of XAS of VO_x films in bleached states (solid lines) and colored states (hollow symbol).

suggesting the atomic rearrangement of these films. The fact that the weight of d_{z^2} is lower in relation to $d_{x^2-y^2}$ in as-deposited VO_x than in AA500 suggests that the central V atom is closer to the basal plane.[34] Therefore, the distance between the central V and vanadyl oxygen is larger, explaining why the d_{z^2} contribution is smaller and the d_{z^2} energy (as observed in the deconvoluted XAS) is lower. Notably, the 3d occupancy number significantly affects the t_{2g} peak, and e_g is closely related to the structural symmetry. The t_{2g} peak from VO_x and AA200 is less intense than in the films that are annealed above 300 °C. Thus, the change in the intensity of the t_{2g} peak, the spectral profile and ΔE confirm not only that V^{4+} is present in the as-deposited VO_x, but also that V^{4+} is present in the form of VO_2 (B). Similarities in the 4sp region support this inference, as shown in Fig. 2(b). The mixture of VO_2 (B) in the O 1s XAS spectra may contribute to the disorder in the film. Therefore, the decrease in the interlayer distance and the FWHM after thermal annealing, as revealed by GIXRD, is related to the rearrangement of the sputtered atoms and the decrease in the amount of VO_2 (B) in the films.

Fig. 4(a) displays the V L-edge XAS of the films following a gasochromic reaction. Inserting hydrogen changes the color of the film and causes its spectral features to undergo a chemical shift to a lower energy; in addition, its line shapes to become more like those of VO_2. The negative shift of the V L-edge with a drop in valence can be understood as being caused by a decrease in the attractive potential of the nucleus and a weakening of the repulsive Coulomb interaction of the core with the other electrons in the compound. When the film adsorbs H_2, the electron may enter the 3d orbital, thereby reducing the V charge state. The additional electron lowers the charge state of the vanadium ions, causing a shift of the main peak of the V L_3-edge to a lower energy. Notably, the L-edge spectrum in the colored state is less intense than the spectrum in the bleached state. This reduction in intensity can be viewed as a drop in the number of 3d-unoccupied states, implying an increase in the charge in the t_{2g} state of the d orbital upon coloration. The calculation of the band structure by C. Hébert *et al.* suggests that a reduction in valence and a change in the structural symmetry influence the crystal-field effect.[40,41] Therefore, the change in intensity also reflects a modification in the relative weight of the *xy*- (in-plane) and *z* (out-of-plane) characteristics of 3d-orbital transitions in C_{4v} symmetry. This modification is owing to a highly anisotropic layered structure of the film. The difference between the 3d band splitting in the bleached and colored films is related to the variations in the structural geometries and electronic configurations, and the subsequent difference between the line profiles of XAS spectra.

Fig. 4(b) presents the corresponding O K-edge. Notably, the most significant change between the colored and bleached states in the O K-edge region is that the intensity of the t_{2g} structure is lower in the colored film than that in the bleached films. This phenomenon reflects the extra electron occupancy in the t_{2g} orbital that is associated with the incorporation of hydrogen atoms. The d-orbital of V^{5+} is formally d^0 ($t_{2g}{}^0e_g{}^0$) and V^{4+} is formally d^1 ($t_{2g}{}^1e_g{}^0$), explaining why the intensity ratio of t_{2g} and e_g is directly related to the 3d orbital occupancy. The drop in t_{2g} of the films upon the gasochromic reaction is caused by the reduction of V^{5+}, and is consistent with the V L-edge. The extra electron occupancy may affect the 3d(t_{2g})-O hybridization, alter the orbital orientation and, ultimately, distort the lattice structure. The above results suggest that the changes in orbital orientation are attributed to the modification of the lattice structure from the distorted O_h-like symmetry (C_{4v}) of the V_2O_5 thin film in the bleached state to the more symmetrical O_h-like structure of the film in the colored state, which correlates well with the V K-edge results.

Unlike the V L-edge that is used primarily to probe V 3d states (atomic in nature), V K-edge spectral features represent transitions from the core levels to 4p-like states that are less localized than the 3d states. Thus, as is expected, the V K-edge provides further insight into energy band dispersion that arises from the solid-state effects by probing the more delocalized levels that are derived from V 4p orbitals. Although sensitive to the valence and the local atomic surroundings of the absorbing element, the features at the V K-edge XAS are also influenced by constructive and destructive interferences (*i.e.* single and multiple scattering) from the neighbors around the central vanadium atoms. Such interferences are caused not only by several electronic many-body effects (*e.g.*, quadrupolar transitions), but also by changes in the medium- and long-range environments. While the main transition at the K-edge is electric dipolar-allowed (1s to 4p), the pre-edge peak area is correlated mainly with the transition from the 1s core level to empty 3d states.[42] The electronic transition in the pre-edge area becomes allowed when the inversion center is lost. In an O_h-like structure, the loss of symmetry allows for partial overlapping and mixing of the unfilled d states of the metal with the 4p orbital of the metal *via* V ligands (2p states).[43] Normally, the pre-edge peak intensity is virtually zero when the symmetry around the absorber is regular octahedral; this intensity is higher when the symmetry is tetrahedral.[44] Therefore, the pre-edge intensity is a clear fingerprint of the change in symmetry. Additionally, this intensity is used to evaluate qualitatively the alteration of the local structure of vanadium. A rather intense pre-edge peak is obtained from the vanadinite with tetrahedral V^{5+}, and the pre-edge peak becomes very weak when the symmetry is regular octahedral, as it does for coulsonite.[44]

Fig. 5(a) and (c) display the V 1s XAS spectra of the films before and after gasochromic reaction. Fig. 5(b) compares these spectra. In the gasochromic reaction, the films are exposed to hydrogen at 101.325 kPa and 25 °C for 2 h. All spectra were obtained at an angle of incidence of 45°. The insets present photographs of the films before and after the gasochromic reaction. According to Fig. 5(a), the spectra of VO_x and AA200 before gasochromic reaction are almost the same, and they converge to the characteristic spectrum of crystalline V_2O_5 at temperatures above 300 °C. According to Fig. 5, the V K-edge is highly sensitive to the local symmetry of the vanadium site. All spectra include a pre-edge A_5, which is well known to be a formally forbidden 1s–3d electronic transition, which becomes dipole-allowed as the full local O_h symmetry is reduced. Two factors influence the pre-peak. First, distortion of the symmetry from O_h tends to significantly enhance the pre-edge intensity.[43,44] Second, the emptiness of the p states in the p–d hybridized orbitals increases as the number of d electrons decreases, subsequently raising the pre-edge peak.[42] Pre-edge A_5 in both VO_x and AA200 is less pronounced than that in the more crystalline AA300 and AA400, owing to the change in the vertical asymmetry of the apical V–O bond, which is confirmed by the results for xerogel, aerogel and cystalline V_2O_5.[45] The pre-peak intensity of crystalline V_2O_5 surpasses that of xerogel and aerogel. Notably, xerogel has V–O apical bonds at 1.58 and 2.31 Å, and aerogel at 1.6 and 2.31 Å.[45] These values differ by less than those of crystalline V_2O_5, which are 1.58 and 2.79 A. This fact explains why the pre-edge peak of VO_x and AA200 has a lower intenstiy. The main feature B_5 is associated with the continuum states and arises from multiple scattering resonances of the photoelectrons. The symmetry of the four basal oxygens that surround the vanadium sites influences the intensity and shape of the edge resonance.[46,47] The intensity and shape of the edge resonance of the VO_x and AA200 differ from those of the crystalline AA300 and AA400, as revealed by peak B_5 in Fig. 5(a). This occurrence follows from a different local structural arrangement of the VO_6 units in VO_x and AA200 from that in crystalline AA300 and AA400.

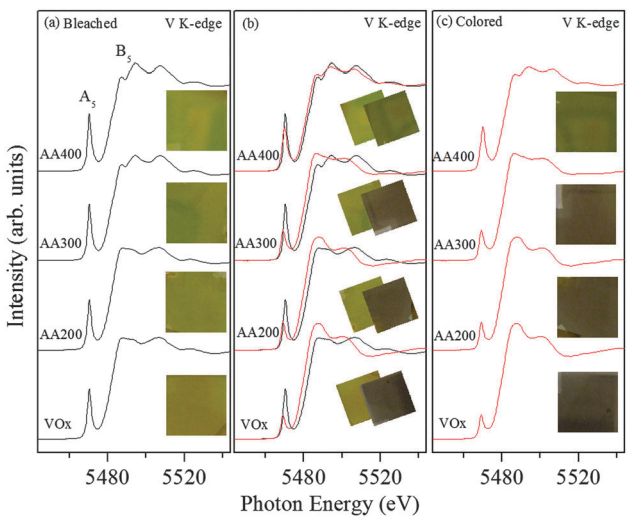

Fig. 5 V K-edge XAS spectra of films (a) before (black lines) and (c) after (red lines) gasochromic reaction. Insets show photographs of films before and after gasochromic reaction. (b) Overlay of (a) and (c) for comparison.

The gasochromic reaction shifts the absorption edge to a lower photon energy and reduces the pre-edge intensity, as displayed in Fig. 5(b). The gasochromic reaction coincides with the change in the color of the film from yellow to gray. The spectral and color changes in AA400 are relatively minor. The color becomes black upon exposure to hydrogen for ~72 h, as discussed in a later section. Peak B_5 following the absorption jump is associated with scattering in the plane of the pyramid base.[46,47] Therefore, the main differences between the films before and after the gasochromic reaction arise from the fact that the rearrangement of the atoms of the base causes less distortion in the colored state than in the bleached state. Peak A_5 originates from the multiple scattering pathways along the axis of the pyramid[43,47] and, therefore, depends on the positions of the apical V–O. Interestingly, the colored states of VO_x and AA200 have markedly different spectral profiles from that of the bleached state. For AA400, the spectral profiles in the colored and bleached states closely resemble each other. However, although the profile of AA300 in the bleached state resembles that of AA400, those in colored states differ from each other, suggesting that color switching is closely related to the amorphous character.

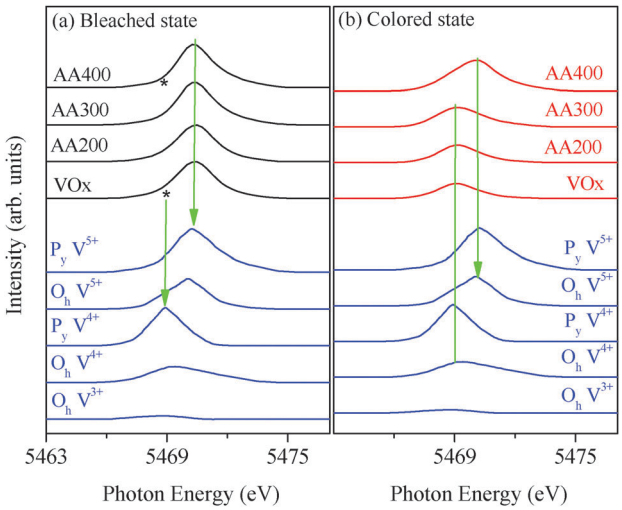

Fig. 6 Pre-edge region of V K-edge XAS of VO_x, AA200, AA300 and AA400 in (a) bleached states and (b) colored states.

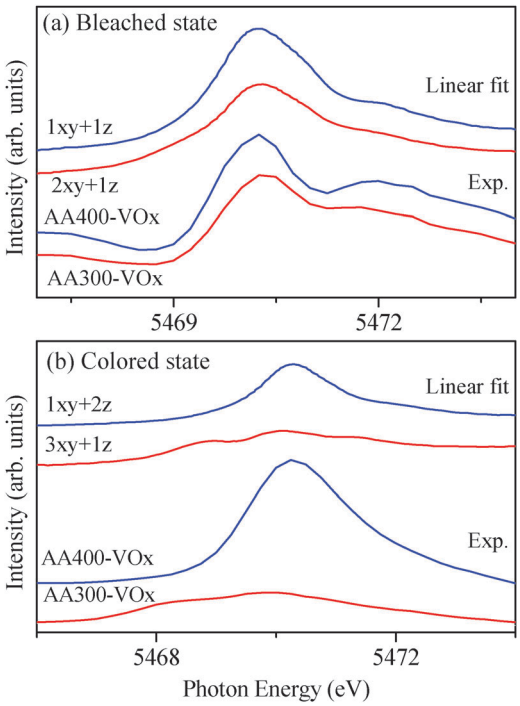

Fig. 7 Experimental spectral differences between VO_x and annealed films and those fitted by linear combination of *xy* and *z* components in (a) bleached states and (b) colored states.

To study the effect on the vanadium oxidation state and/or symmetry upon annealing, the pre-edge feature is extracted and compared with various standard vanadium oxides. The contribution of the pre-peak is obtained by subtraction of the baseline. Fig. 6(a) presents the pre-peak region of the sputtered films along with that of the standards with different crystal symmetries. Clearly, the spectral profiles of all of the films resemble each other and also resemble that of P_y (V^{5+}), indicating that vanadium is most likely in the form of V^{5+} with pyramid symmetry. Notably, the drop in intensity is accompanied by an enhancement of the contribution on the low-energy side (as denoted by the star in Fig. 6(a)), implying the possible presence of pyramidal V^{4+}, which is consistent with the above speculation based on the V L-edge. Fig. 6(b) displays the change in the pre-peak region of the films upon H_2 adsorption. The pre-edge region in Fig. 6(b) demonstrates that for AA400, the charge state of V remains unchanged by the gasochromic reaction, but that the structural symmetry is modified from P_y (V^{5+}) to O_h (V^{5+}), and that for the other films, the structural symmetry is modified from P_y (V^{5+}) to a mixture of P_y (V^{4+}) and O_h (V^{4+}). The above results reveal that in the as-deposited and annealed films (below 300 °C), gasochromism changes not only the charge state but also the symmetry.

Exactly how annealing affects the films is more closely examined. The lower part of Fig. 7(a) presents the spectral differences between VO_x and annealed films in bleached states. Notably, AA200 and VO_x differ negligibly and are thus not considered in Fig. 7. According to the theoretical polarized XAS of V_2O_5, the components along the *z* axis and in the basal plane contribute to the pre-edge region. However, the remarkably intense pre-peak appears only if a short V–O bond is present along the *z*-axis,[43,47] emphasizing the importance of the vanadyl oxygen. The curve that is fitted with a linear combination of the calculated *z*-component and the calculated *xy*-component is compared with the experimental data.[43,47] The fitting curve agrees with the experimental data to some extent (Fig. 7(a)). The ratio of *z*- to *xy*-components in the difference spectra of (AA400-VO_x) and (AA300-VO_x) are 1 : 1 and 1 : 2, respectively. This finding suggests that increasing the thermal annealing temperature shortens the apical V–O bond, explaining why the *z*-component is enhanced. Similarly, an attempt is made to determine how H_2 adsorption affects the films. Fig. 7(b) presents the spectral differences in the color states. The calculations demonstrate that the weights of the *z* and *xy* components are in the ratio 2 : 1 for (AA400-VO_x) and 1 : 3 for (AA300-VO_x). The greater *xy*-component in AA300 implies that the central V atom is forced to move closer to the basal plane upon coloration.

The small changes in the spectral profiles and color indicate that the coloration rate of AA400 declines when the lamellar structure is removed by thermal annealing. Changes in the V 1s XAS spectra suggest that the gasochromic reaction is closely related to a decrease in the oxidation state of vanadium and an increase in its octahedral symmetry. Above results thus reveal that the coloration rate is strongly correlated with the formation of a lamellar structure. Additionally, increasing the annealing temperature increases the weight of the *z*-component, revealing that H_2 adsorption causes structural modulation. The increase in the strength of the *z*-component suggests the importance of the apical oxygen.

Vanadium sites in the V_2O_5 gels are highly asymmetric and the V–O distances vary greatly.[47] While observed in gels on a flat substrate, spontaneous texturation causes strong anisotropy in physical properties.[46] A lamellar structure may provide a channel for the rapid intercalation of ion species in V_2O_5 gels,

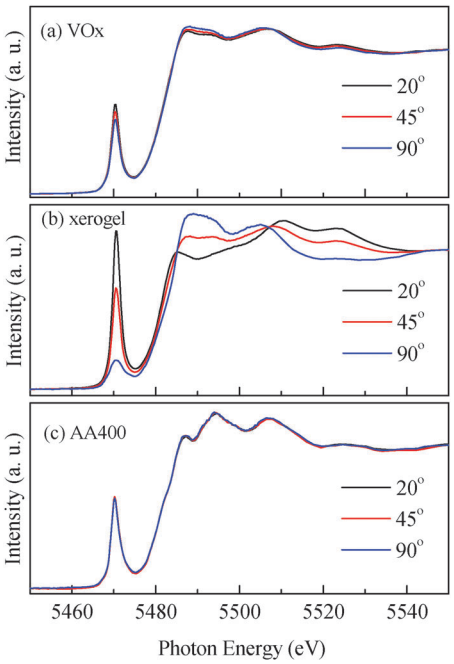

Fig. 8 V polarized K-XAS spectra of (a) as-deposited VO_x, (b) $V_2O_5{\cdot}1.6H_2O$ xerogel, and (c) AA400 film for incidence angles of 20°, 45°, and 90°.

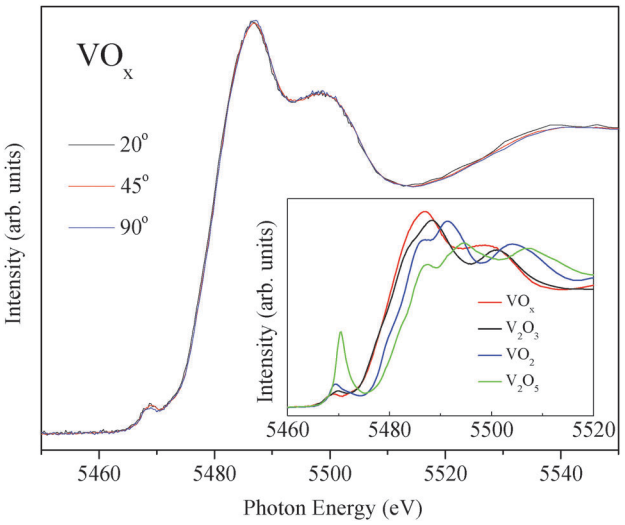

Fig. 9 V polarized K-XAS spectra of hydrogen-saturated VO_x for incidence angles of 20°, 45°, and 90°. Inset shows V K-XAS spectra of hydrogen-saturated VO_x (incidence angle of 45°) and standards (V_2O_3, VO_2 (M), and V_2O_5).

and the formation of a lamellar structure may lead to anisotropy in the film.[28,46] Polarized absorption spectra separate the contributions of neighboring atoms in different directions. K-edge XAS spectra are more prone to solid-state effects (*i.e.* energy band dispersion) and are much more affected by polarization than are L-edge spectra. This study also examined how the lamellar structure affects the intercalation rate and anisotropy in sputtered VO_x by using polarized V K-XAS (Fig. 8(a)). This figure reveals that, with an increasing angle of incidence of X-rays, the pre-edge feature is reduced and the main peak is enhanced. Fig. 8(b) displays the V-polarized K-XAS spectra of oriented $V_2O_5{\cdot}1.6H_2O$ for comparison. As shown in the inset, the spectra vary substantially with the angle of incidence, which is consistent with the literature.[46] Variations of the as-deposited VO_x are smaller than those of $V_2O_5{\cdot}1.6H_2O$ xerogel, and all spectra resemble that of $V_2O_5{\cdot}1.6H_2O$ xerogel at an angle of incidence of 45°. Experimental results indicate that sputtered VO_x films have only weak anisotropy, which is related to the disorder of the lamellar structure. The absence of anisotropy in the V K-edge in AA400 verifies that polycrystallinity is responsible for the weaker anisotropy in the L-edge, as shown in Fig. 8(c).

Gasochromic material must behave reliably and repeatedly if it is to be used in practice. Consequently, the failure of a film of such material should be examined to more thoroughly understand it and to help engineer the material. Therefore, in this study, an *in situ* experiment is performed on films in a sample holder filled with hydrogen to prevent the out-diffusion of hydrogen during data collection. The films are exposed continuously to hydrogen until they are hydrogen-saturated; all films become black after ~72 h. Hydrogen-saturated VO_x is then studied using *in situ* polarized V K-XANES. Fig. 9 shows the spectra that were obtained using three experimental geometries. Clearly, the spectra resemble each other and no anisotropic effect is observed in the hydrogen-saturated VO_x film.

The inset in Fig. 9 compares the V K-XAS spectra of hydrogen-saturated VO_x with those of the references (V_2O_3, VO_2, and V_2O_5). The main absorption edge of the hydrogen-saturated VO_x significantly overlaps that of the V_2O_3 standard, revealing that the vanadium valence is approximately +3. Many vanadium-based electrochromism/gasochromism-related studies have described the transformation of pentavalent to tetravalent vanadium by the gasochromic reaction.[48] Trivalent vanadium has seldom been examined, yet has been found in $Li_xV_2O_5$[26] and $H_xV_2O_5$.[49] The presence of trivalent vanadium in the VO_x film may be attributed to the over-reaction of the film with hydrogen during coloration. The overlapping V-polarized K-XAS spectra reveal that hydrogen-saturated VO_x is isotropic, indicating that the gasochromic reaction equalizes the V–O distances, subsequently lowering the distortion and increasing the octahedral symmetry in the films. Additionally, the inter-diffusion of hydrogen atoms reduces the interlayer distance and reduces the lamellar character of the structure. The elimination of anisotropy is probably related to the increased octahedral symmetry and the breaking up of the lamellar structure. Upon coloration, the hydrogen diffuses into the interlayer. Owing to the large interlayer space, small ions like hydrogen can move freely in the lamellar structure. However, excessive gasochromism causes an excess of hydrogen in the structure; this hydrogen is very likely irreversible in forming the H_xVO_y phase.

The structures of the hydrogen-saturated films are studied using XRD. Fig. 10 presents the results. Unlike AA300 and AA400 (whose XRD spectra are shown in Fig. 1), AA300 and AA400 in hydrogen-saturated films yield no peak that corresponds to the orthorhombic V_2O_5 phase. Instead, tiny phase transitions to the $H_{1.43}V_2O_5$ phase are found in the films. The small peak at 28.4° cannot be identified. The inset shows the GIXRD patterns of

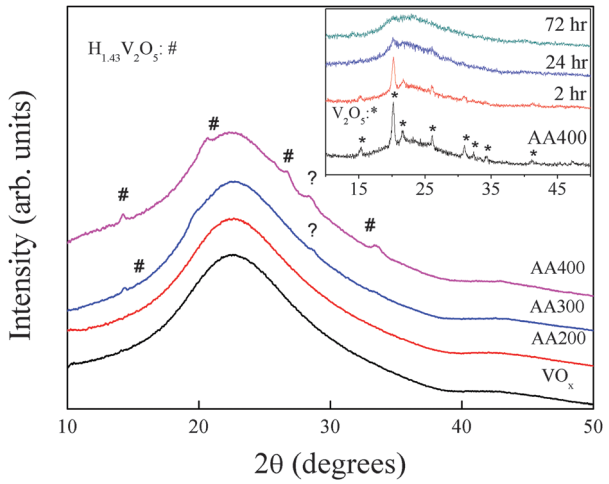

Fig. 10 XRD patterns of as-deposited and annealed VO_x films after exposure to hydrogen for 72 h. Inset shows GIXRD patterns of AA400 as a function of exposure time to hydrogen.

AA400 for various durations of exposure to hydrogen. The inset reveals an amorphization process, in which the peaks that correspond to orthorhombic become V_2O_5 progressively weaker with an increasing exposure time, and disappear by 72 h. Moreover, the phase transition is not found in as-deposited VO_x and AA200, suggesting that VO_x and AA200 are highly promising for gasochromic applications.

As is generally accepted the color change that occurs upon the intercalation of hydrogen is caused by a change in the valence of the cation. However, its mechanism remains unclear. According to our results, the intercalation of hydrogen causes a considerable structural rearrangement and a large change in bonding in the orthorhombic V_2O_5. Additionally, the difference between the amorphous VO_x and orthorhombic V_2O_5 crystalline phase is related to intrinsic structural differences. As is widely assumed, the stereochemistry of crystalline orthorhombic V_2O_5 is determined by deformed octahedral VO_6, which serves as the building block of the V_2O_5 structure. The deformed VO_6 octahedra form warped layers that are connected to each other by V═O–V bridges of length 4.37 Å.[50] Only weak van der Waals interactions are assumed to exist between the layers. Moreover, the intercalated hydrogen attaches to the oxide matrix to form –OH groups[51] or $–OH_2$ groups.[52] No evidence of metal–hydrogen bonds is available. Also, hydrogen forms $–OH_2$ groups at the apices of the square pyramid that surrounds each vanadium ion.[52] Correspondingly, the layered structure of V_2O_5 is broken and the V═O–V bridges can no longer be established. The breaking up of chemical bonds subsequently causes a phase transformation into another stable phase, such as $H_{1.43}V_2O_5$. According to related studies, amorphous V_2O_5 gels have a ribbon-like structure that comprises two V_2O_5 sheets facing each other at a distance of 2.8 Å.[30–32] The structure resembles that of the layered phase of $Ag_xV_2O_5$, in which the vanadyl oxygen does not form a chemical bond with another layer. The intercalated hydrogen may attach only to the vanadyl oxygen without significantly affecting the chemical bonding. Hence, no phase transformation is observed in the amorphous V_2O_5. Without knowledge of the fundamental electronic and atomic structures of the gasochromic films and the changes of those structures upon the adsorption of H_2, better engineering of the film for more practical purposes is impossible. Growth parameters must be finely tuned to optimize the thin film. The XAS spectrum is exploited herein as an indicator of the overall gasochromic properties of sputtered films. Moreover, we recommend using a film with a small amount of V^{4+} and a lamellar structure for applications. Above results significantly contribute to efforts to develop a reliable and inexpensive hydrogen sensor technology, which is critical to ushering in a hydrogen economy.

Summary

VO_x thin films with lamellar structures were successfully prepared by sputter deposition. The geometric and electronic structures of these smart films were characterized by XAS measurements at the V K-edge, V L-edge and O K-edge. XAS lineshapes, peak positions, and intensities yield valuable information on the local electronic structure, the transition metal oxidation state, the ligand type, and site symmetry. The films had a V^{4+} and V^{5+} mixed valence, and V^{4+} was present in the form of VO_2 (B). Analytical results indicate that the intercalation of sputtered species and the mixing of VO_2 (B) are responsible for the disordered and expanded lamellar structure. The gasochromic reaction causes films with the orthorhombic V_2O_5 crystalline phase to undergo an amorphization process and a partial transformation into an irreversible $H_{1.43}V_2O_5$ phase. Additionally, the gasochromic reaction reduces the vanadium valence and alters the as-deposited VO_x from slightly anisotropic to isotropic. The gasochromic rate is strongly correlated with the lamellar structure. Color switching upon the intercalation of hydrogen is not only caused by the valence change of the cations, but also accompanied by the local atomic rearrangement. Much of the physics of this mechanism remains to be explored. Our results further demonstrate that the local atomic structure significantly influences the gasochromism. Owing to its stable structure and a high coloration rate, amorphous VO_x film with a lamellar structure is recommended for use in H_2 gas sensors. Results of this study significantly contribute to efforts to improve the reaction rate and durability of vanadium-oxide-based hydrogen sensors by elucidating their atomic and electronic structures.

Acknowledgements

This study was financially supported by the National Science Council of Taiwan under grants NSC 101-2112-M-213-004-MY3, 102-2112-M-001-004-MY3, 99-2221-E-024-003, and 97-2221-E-006-006-MY3.

References

1 C. G. Granqvist, A. Azens, P. Heszler, L. B. Kish and L. Österlund, *Sol. Energy Mater. Sol. Cells*, 2007, **91**, 355–365.
2 C. G. Granqvist, *Nat. Mater.*, 2006, **5**, 89–90.
3 C. G. Granqvist, *Adv. Mater.*, 2003, **15**, 1789–1803.

4 M. Gratzel, *Nature*, 2001, **414**, 338–344.
5 I. L. T. M. S. Dresselhaus, *Nature*, 2001, **414**, 332–337.
6 H. Nakagawa, N. Yamamoto, S. Okazaki, T. Chinzei and S. Asakura, *Sens. Actuators, B*, 2003, **93**, 468–474.
7 M. Ranjbar, S. M. Mahdavi and A. Iraji zad, *Sol. Energy Mater. Sol. Cells*, 2008, **92**, 878–883.
8 M. Ranjbar, A. Iraji zad and S. M. Mahdavi, *J. Phys. D: Appl. Phys.*, 2008, **41**, 055405.
9 J. Liu, H. Xia, D. Xue and L. Lu, *J. Am. Chem. Soc.*, 2009, **131**, 12086–12087.
10 A.-M. Cao, J.-S. Hu, H.-P. Liang and L.-J. Wan, *Angew. Chem., Int. Ed.*, 2005, **44**, 4391–4395.
11 P. Liu, S.-H. Lee, H. M. Cheong, C. E. Tracy, J. R. Pitts and R. D. Smith, *J. Electrochem. Soc.*, 2002, **149**, H76.
12 C. L. Chen, C. L. Dong, Y. K. Ho, C. C. Chang, D. H. Wei, T. C. Chan, J. L. Chen, W. L. Jang, C. C. Hsu, K. Kumar and M. K. Wu, *Europhys. Lett.*, 2013, **101**, 17006.
13 W.-L. Jang, Y.-M. Lu, Y.-R. Lu, C.-L. Chen, C.-L. Dong, W.-C. Chou, J.-L. Chen, T.-S. Chan, J.-F. Lee, C.-W. Pao and W.-S. Hwang, *Thin Solid Films*, 2013, **544**, 448–451.
14 Y. K. Ho, C. C. Chang, D. H. Wei, C. L. Dong, C. L. Chen, J. L. Chen, W. L. Jang, C. C. Hsu, T. S. Chan, K. Kumar, C. L. Chang and M. K. Wu, *Thin Solid Films*, 2013, **544**, 461–465.
15 Z. Wang, J. Chen and X. Hu, *Thin Solid Films*, 2000, **375**, 238–241.
16 Y. Fujita, K. Miyazaki and C. Tatsuyama, *Jpn. J. Appl. Phys.*, 1985, **24**, 1082–1086.
17 J. Livage, *Chem. Mater.*, 1991, **3**, 578–593.
18 Y. S. Yoon, J. S. Kim and S. H. Choi, *Thin Solid Films*, 2004, **460**, 41–47.
19 H. Shanak, H. Schmitt, J. Nowoczin and K.-H. Ehses, *J. Mater. Sci.*, 2005, **40**, 3467–3474.
20 C. Imawan, H. Steffes, F. Solzbacher and E. Obermeier, *Sens. Actuators, B*, 2001, **77**, 346–351.
21 N. Fateh, G. A. Fontalvo and C. Mitterer, *J. Phys. D: Appl. Phys.*, 2007, **40**, 7716–7719.
22 L. Ottaviano, A. Pennisi, F. Simone and A. M. Salvi, *Opt. Mater.*, 2004, **27**, 307–313.
23 C.-C. Chan, W.-C. Hsu, C.-C. Chang and C.-S. Hsu, *Sens. Actuators, B*, 2011, **157**, 504–509.
24 K. Takahashi, Y. Wang and G. Cao, *Appl. Phys. Lett.*, 2005, **86**, 053102.
25 M. H. Yaacob, M. Breedon, K. Kalantar-zadeh and W. Wlodarski, *Sens. Actuators, B*, 2009, **137**, 115–120.
26 S. Passerini, W. H. Smyrl, M. Berrettoni, R. Tossici, M. Rosolen, R. Marassi and F. Decker, *Solid State Ionics*, 1996, **90**, 5–14.
27 J. Livage, N. Gharbi, M. C. Leroy and M. Michaud, *Mater. Res. Bull.*, 1978, **13**, 1117–1124.
28 G. S. Zakharova and V. L. Volkov, *Russ. Chem. Rev.*, 2003, **74**, 311–325.
29 L.-J. Meng, R. A. Silva, H.-N. Cui, V. Teixeira, M. P. dos Santos and Z. Xu, *Thin Solid Films*, 2006, **515**, 195–200.
30 T. Yao, Y. Oka and N. Yamamoto, *Mater. Res. Bull.*, 1992, **27**, 669–675.
31 M. Giorgetti, S. Passerini, W. H. Smyrl and M. Berrettoni, *Inorg. Chem.*, 2000, **39**, 1514–1517.
32 V. Petkov, P. N. Trikalitis, E. S. Bozin, S. J. L. Billinge, T. Vogt and M. G. Kanatzidis, *J. Am. Chem. Soc.*, 2002, **124**, 10157–10162.
33 C. Zou, L. Fan, R. Chen, X. Yan, W. Yan, G. Pan, Z. Wu and W. Gao, *CrystEngComm*, 2012, **14**, 626.
34 J. M. Velazquez, C. Jaye, D. A. Fischer and S. Banerjee, *J. Phys. Chem. C*, 2009, **113**, 7639–7645.
35 G. Fronzoni, R. De Francesco and M. Stener, *J. Chem. Phys.*, 2012, **137**, 224308.
36 D. Maganas, M. Roemelt, M. Hävecker, A. Trunschke, A. Knop-Gericke, R. Schlögl and F. Neese, *Phys. Chem. Chem. Phys.*, 2013, **15**, 7260–7276.
37 C. W. Zou, X. D. Yan, J. Han, R. Q. Chen and W. Gao, *J. Phys. D: Appl. Phys.*, 2009, **42**, 145402.
38 C. J. Patridge, C. Jaye, H. Zhang, A. C. Marschilok, D. A. Fischer, E. S. Takeuchi and S. Banerjee, *Inorg. Chem.*, 2009, **48**, 3145–3152.
39 R. Mossanek, A. Mocellin, M. Abbate, B. Searle, P. Fonseca and E. Morikawa, *Phys. Rev. B: Condens. Matter Mater. Phys.*, 2008, **77**, 075118.
40 C. Hébert, M. Willinger, D. S. Su, P. Pongratz, P. Schattschneider and R. Schlögl, *Eur. Phys. J. B*, 2002, **28**, 407–414.
41 G. Zhang, G. Woods, E. Shirley, T. Callcott, L. Lin, G. Chang, B. Sales, D. Mandrus and J. He, *Phys. Rev. B: Condens. Matter Mater. Phys.*, 2002, **65**, 165107.
42 J. Wong, R. P. Messmer and D. H. Maylotte, *Phys. Rev. B: Condens. Matter Mater. Phys.*, 1984, **30**, 5596–5610.
43 T. Yamamoto, *X-Ray Spectrom.*, 2008, **37**, 572–584.
44 J. R. Perrine Chaurand, V. Briois, M. Salome, O. Proux, L. O. Vivian Nassif, J. Susini, J.-L. Hazemann and J.-Y. Bottero, *J. Phys. Chem. B*, 2007, **111**, 5101–5110.
45 M. Gioregetti, M. Berrettoni, S. Passerini and W. H. Smyrl, *Electrochim. Acta*, 2002, **47**, 3163–3169.
46 S. Stizza, G. Mancini, M. Benfatto, C. Natoli, J. Garcia and A. Bianconi, *Phys. Rev. B: Condens. Matter Mater. Phys.*, 1989, **40**, 12229–12236.
47 O. Sipr, A. Simunek, S. Bocharov, T. Kirchner and G. Drager, *Phys. Rev. B: Condens. Matter Mater. Phys.*, 1999, **60**, 14115–14127.
48 C. J. Patridge, T.-L. Wu, C. Jaye, B. Ravel, E. S. Takeuchi, D. A. Fischer, G. Sambandamurthy and S. Banerjee, *Nano Lett.*, 2010, **10**, 2448–2453.
49 A. M. Chippindale and P. G. Dickens, *Solid State Ionics*, 1987, **23**, 183–188.
50 C. V. Ramana, O. M. Hussain, B. S. Naidu and P. J. Reddy, *Thin Solid Films*, 1997, **305**, 219–226.
51 P. G. Dickens, A. H. Chlpplndale, S. J. Hibble and P. Lancaster, *Mater. Res. Bull.*, 1984, **19**, 319–324.
52 G. C. Bond, P. A. Sermon and C. J. Wright, *Mater. Res. Bull.*, 1984, **19**, 701–704.

